Charged anisotropic matter with linear or nonlinear equation of state

Victor Varela[*]

Institute of Mathematics, Kings College, University of Aberdeen, Aberdeen AB24 3UE, United Kingdom

Farook Rahaman[†]

Department of Mathematics, Jadavpur University, Kolkata 700 032, West Bengal, India

Saibal Ray[‡]

Department of Physics, Government College of Engineering and Ceramic Technology, Kolkata 700 010, West Bengal, India

Koushik Chakraborty[§]

Department of Physics, Government Training College, Hooghly 712103, India

Mehedi Kalam[‖]

[1]*Department of Physics, Netaji Nagar College for Women, Kolkata 700092, India*

Ivanov pointed out substantial analytical difficulties associated with self-gravitating, static, isotropic fluid spheres when pressure explicitly depends on matter density. Simplifications achieved with the introduction of electric charge were noticed as well. We deal with self-gravitating, charged, anisotropic fluids and get even more flexibility in solving the Einstein-Maxwell equations. In order to discuss analytical solutions we extend Krori and Barua's method to include pressure anisotropy and linear or nonlinear equations of state. The field equations are reduced to a system of three algebraic equations for the anisotropic pressures as well as matter and electrostatic energy densities. Attention is paid to compact sources characterized by positive matter density and positive radial pressure. Arising solutions satisfy the energy conditions of general relativity. Spheres with vanishing net charge contain fluid elements with unbounded proper charge density located at the fluid-vacuum interface. Notably the electric force acting on these fluid elements is finite, although the acting electric field is zero. Net charges can be huge ($10^{19}C$) and maximum electric field intensities are very large (10^{23}–10^{24} statvolt/cm) even in the case of zero net charge. Inward-directed fluid forces caused by pressure anisotropy may allow equilibrium configurations with larger net charges and electric field intensities than those found in studies of charged isotropic fluids. Links of these results with charged strange quark stars as well as models of dark matter including massive charged particles are highlighted. The van der Waals equation of state leading to matter densities constrained by cubic polynomial equations is briefly considered. The fundamental question of stability is left open.

I. INTRODUCTION

Self-gravitating fluid models are essential to many applications of general relativity, ranging from the historically important classical models of elementary particles to current computational and observational problems in astrophysics and cosmology. These systems are usually characterized by sets of physical variables which outnumber the independent field equations. Consistent problems can be posed if additional restrictions on the variables are specified, which may take the form of equations of state (EOS).

Using an EOS to describe a self-gravitating fluid has important consequences when it comes to solving the field equations. For example, Ivanov [1] has pointed out that finding analytical solutions in the static, spherically symmetric, uncharged case of a perfect fluid with linear EOS is an extremely difficult problem.

Interestingly, analytical difficulties may alleviate with increasing physical complexity. This situation has been illustrated by Sharma and Maharaj [2] in the case of a static, spherically symmetric, uncharged anisotropic fluid. These authors chose a particular mass function to reduce and easily solve the system of field equations combined with a linear EOS.

The surprising simplification of the field equations for a charged perfect fluid satisfying a linear EOS was discussed by Ivanov [1], who showed how to reduce the system involving the most general linear EOS to a linear differen-

[*]victor.varela.abdn@gmail.com
[†]farook_rahaman@yahoo.com
[‡]saibal@iucaa.ernet.in
[§]kchakraborty28@yahoo.com
[‖]mehedikalam@yahoo.co.in

tial equation for one metric component. However, Ivanov also pointed out that the use of a polytropic EOS leads to nonintegrable equations.

Electrically charged fluids with anisotropic pressures constitute the next level of physical complexity.

Charged, self-gravitating anisotropic fluid spheres have been investigated in general relativity since the pioneering work of Bonnor [3]. Recently, this type of charged matter has been considered by Horvat, Ilijić, and Marunović in studies of gravastars [4]. Models with prescribed EOS remain relatively unexplored.

Motivated by MIT bag models of strange stars, Thirukkanesh and Maharaj [5] derived solutions for charged anisotropic fluids with linear EOS from specific choices of one metric function and the electrostatic energy density. Their method—an extension of the procedure presented in [2] for uncharged anisotropic fluids-provides motivation for the completely different approach developed in this paper.

Current dark matter and dark energy models are associated with nonlinear EOS. Density perturbations may lead to fluid nucleation characterized by heterogeneous matter densities and pressures. Assuming specific EOS, bounded static fluid distributions and asymptotically flat spacetimes, we aim to study the arising self-gravitating objects. We insist on analytical solutions and note that prescribed EOS may cause serious trouble. However, we find that the convenient choice of a ''frozen'' internal metric reduces the Einstein-charged fluid equations to a system of linear algebraic equations for matter and electrostatic energy densities as well as anisotropic pressures. In a way, we are led to the simplest solution method available for this type of source with prescribed EOS and asymptotically flat spacetime. Models based on linear and nonlinear EOS are completely solved following essentially the same procedure. Remarkably, our approach uncovers the effects of different EOS on hydrostatic and electrical variables without interfering changes of internal metric (apart from adjustable numerical factors depending on junction conditions). This treatment offers a fresh view of the relationships among EOS, charge distributions and pressure anisotropy.

In Sec. II we write the field equations and briefly review the work of Thirukkanesh and Maharaj. Also, the original Krori and Barua solution method is generalized to deal with charged anisotropic sources with regular interiors. Our approach to linear and nonlinear EOS leading to models with positive definite matter density is presented in Sec. III. In Sec. IV we discuss junction conditions and reformulate our procedure in terms of dimensionless quantities. Section V includes a detailed analysis of models with positive matter density and positive radial pressure, paying special attention to conditions for physical acceptability as well as equilibrium conditions and the values of key physical parameters in Gaussian-cgs units. In Sec. VI we specu-

late on the origin of charge in models with linear and nonlinear EOS, and check our solution method against a more complicated EOS describing quintessence stars. Finally, we suggest avenues for further research involving stability analysis and gravitational collapse.

II. CHARGED ANISOTROPIC MATTER

The starting point is the static, spherically symmetric line element represented in curvature coordinates. It reads

$$ds^2 = e^\nu dt^2 - e^\lambda dr^2 - r^2 d\theta^2 - r^2 \sin^2\theta d\phi^2, \quad (1)$$

where $\nu = \nu(r)$ and $\lambda = \lambda(r)$. For the static, charged source with density $\rho = \rho(r)$, radial pressure $p_r = p_r(r)$, tangential pressure $p_t = p_t(r)$, proper charge density $\sigma = \sigma(r)$, and electric field $E = E(r)$ the Einstein-Maxwell (EM) equations take the form

$$8\pi\rho + E^2 = e^{-\lambda}\left(\frac{\lambda'}{r} - \frac{1}{r^2}\right) + \frac{1}{r^2}, \quad (2)$$

$$8\pi p_r - E^2 = e^{-\lambda}\left(\frac{\nu'}{r} + \frac{1}{r^2}\right) - \frac{1}{r^2}, \quad (3)$$

$$8\pi p_t + E^2 = \frac{e^{-\lambda}}{2}\left(\nu'' + \frac{\nu'^2}{2} + \frac{\nu' - \lambda'}{r} - \frac{\nu'\lambda'}{2}\right), \quad (4)$$

$$\sigma = \frac{e^{-(\lambda/2)}}{4\pi r^2}(r^2 E)', \quad (5)$$

where the primes denote differentiation with respect to r, and geometrized units ($G = c = 1$) are employed.

Equations (2)–(5) are invariant under the transformation $E \to -E$, $\sigma \to -\sigma$. In this work we exclusively deal with the positive square root of E^2.

With our choice of radial coordinate, the metric function e^λ and electrostatic energy density E^2 assumed in [5] take the forms

$$e^\lambda = \frac{1 + ar^2}{1 + (a - b)r^2}, \quad (6)$$

$$E^2 = \frac{k(3 + ar^2)}{(1 + ar^2)^2}, \quad (7)$$

where a, b, k are arbitrary constants.

The combination of (6) and (7) with (2) yields

$$\rho = \frac{(b - k)(3 + ar^2)}{8\pi(1 + ar^2)^2}. \quad (8)$$

Hence ρ and E^2 are proportional when $k \neq 0$ and $k \neq b$. This expression for $\rho(r)$ is joined to a linear EOS to provide $p_r(r)$. The explicit form of $p_r(r)$ together with (6), (7), and (3) imply a linear differential equation for $\nu(r)$ which is analytically solved. Finally, when (6) and (7) and the explicit form of $\nu(r)$ are substituted into (4) we get the corresponding expression for $p_t(r)$.

The above procedure leads to analytical solutions which depend on a number of free parameters. The analysis presented in [5] considers sensible choices for these parameters in the context of charged stars. However, we find a singularity in the charge distribution at $r = 0$ when (6) and (7) are combined with (5).

From (6) we see that $\lambda(r)$ satisfies $\lambda(0) = 0$. Assuming $k > 0$, (5) implies

$$\sigma(r) \approx \frac{\sqrt{3k}}{2\pi} \frac{1}{r} \qquad (9)$$

for small r, which diverges at $r = 0$. The electric field associated with (7) does not vanish at $r = 0$. This choice for $E(r)$ prevents the regularity of the charge distribution at the center of the sphere.

In our view, the vanishing of the electric field at the center of a spherically symmetric charge distribution should be a condition for physical relevance of the solution. Furthermore the significance of charge density singularities is unclear and we aim to investigate their possible occurrence in models satisfying $E(0) = 0$. To this end, we extend Krori and Barua's approach to charged isotropic fluid sources [6] and deal with charged anisotropic sources with prescribed EOS.

Krori and Barua (KB) constructed singularity-free models of static, charged perfect fluids with metric (1) given by

$$\lambda = Ar^2, \qquad (10)$$

$$\nu = Br^2 + C, \qquad (11)$$

where A, B, and C are constants. This internal metric satisfies the conditions for regularity at $r = 0$ discussed by Lake and Musgrave [7]. As a consequence of this choice, Eqs. (2)–(4) with $p_r = p_t = p$ were reduced to a system of three linear algebraic equations for ρ, p, and E^2. Furthermore σ was obtained combining (5) with the chosen square root of E^2 and the assumed form of λ.

We rewrite the field equations as

$$8\pi\rho + E^2 = f(r), \qquad (12)$$

$$8\pi p_r - E^2 = h(r), \qquad (13)$$

$$8\pi p_t + E^2 = j(r), \qquad (14)$$

where $f(r)$, $h(r)$, $j(r)$ are determined by the right sides of (2)–(4), (10), and (11), namely

$$f(r) = e^{-Ar^2}\left(2A - \frac{1}{r^2}\right) + \frac{1}{r^2}, \qquad (15)$$

$$h(r) = e^{-Ar^2}\left(2B + \frac{1}{r^2}\right) - \frac{1}{r^2}, \qquad (16)$$

$$j(r) = e^{-Ar^2}[B + B^2r^2 + (B - A) - ABr^2]. \qquad (17)$$

We impose center and boundary conditions on $E(r)$ and $p_r(r)$, respectively:

$$E(0) = 0, \qquad (18)$$

$$p_r(a) = 0, \qquad (19)$$

where a is a positive constant and $r = a$ defines the charged fluid-vacuum interface.

From (12)–(19), we obtain

$$8\pi\rho(0) = 3A, \qquad (20)$$

$$4\pi\rho(a) = (A + B)e^{-a^2A}, \qquad (21)$$

$$8\pi p_r(0) = 2B - A, \qquad (22)$$

$$8\pi p_t(0) = 2B - A, \qquad (23)$$

$$8\pi p_t(a) = e^{-a^2A}\left[4B - A + a^2(B^2 - AB) + \frac{1}{a^2}\right] - \frac{1}{a^2}, \qquad (24)$$

$$E^2(a) = \frac{1}{a^2} - e^{-a^2A}\left(2B + \frac{1}{a^2}\right). \qquad (25)$$

From (22) and (23), we conclude that only one pressure value is associated with $r = 0$. Hence $p_r(0)$ and $p_t(0)$ denote the same quantity i.e. central pressure.

Equations (12)–(14) yield general expressions for p_t and E^2 namely

$$p_t = \frac{j(r) - f(r)}{8\pi} + \rho, \qquad (26)$$

$$E^2 = f(r) - 8\pi\rho, \qquad (27)$$

where ρ is still undetermined.

III. LINEAR OR NONLINEAR EQUATION OF STATE

At this point we select an EOS with the general form

$$p_r = p_r(\rho, \alpha_1, \alpha_2), \qquad (28)$$

where α_1 and α_2 are constant parameters.

These parameters are constrained by the system of equations

$$p_r(0) = p_r[\rho(0), \alpha_1, \alpha_2], \qquad (29)$$

$$0 = p_r[\rho(a), \alpha_1, \alpha_2]. \qquad (30)$$

Combining (12) and (13) we get

$$\rho + p_r = \frac{f(r) + h(r)}{8\pi}, \qquad (31)$$

which may be solved with the assumed EOS to generate

specific forms of ρ and p_r. The arising ρ is put into (26) and (27) to yield general expressions for p_t and E^2.

First, we consider the linear EOS

$$p_r = \alpha_1 + \alpha_2 \rho. \qquad (32)$$

Following the outlined procedure we obtain

$$\rho = \frac{\frac{1}{8\pi}[f(r) + h(r)] - \alpha_1}{1 + \alpha_2}, \qquad (33)$$

$$p_r = \frac{\alpha_1 + \frac{\alpha_2}{8\pi}[f(r) + h(r)]}{1 + \alpha_2}, \qquad (34)$$

$$p_t = \frac{j(r) + h(r) + \alpha_2[j(r) - f(r)] - 8\pi\alpha_1}{8\pi(1 + \alpha_2)}, \qquad (35)$$

$$E^2 = \frac{8\pi\alpha_1 + \alpha_2 f(r) - h(r)}{1 + \alpha_2}. \qquad (36)$$

Taking into account (32) we solve the system (29) and (30) and get

$$\alpha_1 = -\frac{\rho(a)p_r(0)}{\rho(0) - \rho(a)}, \qquad \alpha_2 = \frac{p_r(0)}{\rho(0) - \rho(a)}. \qquad (37)$$

Second, we deal with the nonlinear EOS

$$p_r = \beta_1 + \frac{\beta_2}{\rho^n}, \qquad (38)$$

where $n \neq -1$. Combining (38) with (31) we obtain a polynomial equation for ρ which is quadratic only for $n = -2$ or $n = 1$. The second choice for n yields

$$\rho = \frac{k(r) - \beta_1 \pm \sqrt{[k(r) - \beta_1]^2 - 4\beta_2}}{2}, \qquad (39)$$

where

$$k(r) = \frac{f(r) + h(r)}{8\pi}. \qquad (40)$$

Solving (29) and (30) with (38) and $n = 1$ we get

$$\beta_1 = \frac{\rho(0)p_r(0)}{\rho(0) - \rho(a)}, \qquad \beta_2 = -\frac{\rho(0)\rho(a)p_r(0)}{\rho(0) - \rho(a)}. \qquad (41)$$

If $\beta_2 < 0$ then each root in (39) has definite sign. Particularly, the root with the positive radical determines a positive definite matter density.

Equation (38) is a modification of the Chaplygin gas EOS used by Bertolami and Páramos to describe neutral dark stars [8]. Actually, the Chaplygin gas EOS is polytropic with negative polytropic index. The additional term β_1 allows for a charged fluid-vacuum interface where $p_r = 0$.

Third, we consider the modified Chaplygin EOS

$$p_r = \gamma_1 \rho + \frac{\gamma_2}{\rho} \qquad (42)$$

used in the study of static, neutral, phantomlike sources presented by Jamil, Farooq, and Rashid [9].

Equations (29) and (30) combined with (42) yield

$$\gamma_1 = \frac{\rho(0)p_r(0)}{\rho(0)^2 - \rho(a)^2}, \qquad \gamma_2 = -\frac{\rho(0)p_r(0)\rho(a)^2}{\rho(0)^2 - \rho(a)^2}. \qquad (43)$$

Putting (42) into (31) we get a quadratic equation for ρ which admits the solutions

$$\rho = \frac{k(r) \pm \sqrt{k(r)^2 - 4(1 + \gamma_1)\gamma_2}}{2(1 + \gamma_1)}. \qquad (44)$$

If $1 + \gamma_1 > 0$ and $\gamma_2 < 0$ then the sign of the radical in (44) uniquely determines the sign of ρ. As in the previous case, a positive radical leads to positive definite matter density.

Finally, the expressions for ρ selected from (39) and (44) are combined with the corresponding EOS as well as (26) and (27) to yield solutions for p_r, p_t, and E^2.

It is clear that the constant parameters appearing in (28) play a central role in our extension of the KB method. Their values determine the existence of positive and negative definite matter densities $\rho(r)$. Furthermore, they lead to numerical values for quantities like $\frac{dp_r}{d\rho}$, which is associated with sound propagation in anisotropic charged fluids [10].

IV. JUNCTION CONDITIONS AND ADIMENSIONAL FORMULATION

Equations (37), (41), and (43) show that the constant parameters are determined by $\rho(0)$, $\rho(a)$ and $p_r(0)$, which, according to (20) and (22), are functions of the KB constants A and B appearing in (10) and (11). Notably, these two constants as well as C are fixed by suitable junction conditions imposed on the internal and external metrics at $r = a$.

The external Reissner-Nordström (RN) metric is given by (1) with

$$e^{\nu(r)} = 1 - \frac{2m}{r} + \frac{q^2}{r^2}, \qquad e^{\lambda(r)} = \left[1 - \frac{2m}{r} + \frac{q^2}{r^2}\right]^{-1}. \qquad (45)$$

Junevicus [11] derived expressions for A, B, C from the continuity of the first and second fundamental forms across the surface of the charged fluid sphere. In terms of the dimensionless parameters $\mu = \frac{m}{a}$ and $\chi = \frac{|q|}{a}$ his results take the form

$$A = -\frac{1}{a^2} \ln(1 - 2\mu + \chi^2), \qquad (46)$$

$$B = \frac{1}{a^2}\left(\frac{\mu - \chi^2}{1 - 2\mu + \chi^2}\right), \qquad (47)$$

$$C = \frac{\chi^2 - \mu}{1 - 2\mu + \chi^2} + \ln(1 - 2\mu + \chi^2). \quad (48)$$

Combining (25) with (46) and (47) we obtain the electrostatic energy density at the surface of the sphere, namely,

$$E(a)^2 = \frac{q^2}{a^4}. \quad (49)$$

On the other hand, using (45) in the electrovac ($\rho = 0$) case of (2) we see that the same quantity evaluated in the external ($r > 0$) spacetime region is

$$E(r)^2 = \frac{q^2}{r^4}. \quad (50)$$

These results are compatible with the continuity of the electric field at $r = a$.

For simplicity in numerical calculations, we reformulate our results in terms of dimensionless quantities. From (10) and (11) we see that A, B have dimension of length^{-2} whereas C is dimensionless. Clearly $f(r)$, $h(r)$, $j(r)$ as well as ρ, p_r, p_t, E^2, σ also have dimension of length^{-2}. We get the dimensionless version of any variable or constant parameter multiplying by the appropriate power of a. Here adimensionality is denoted by tildes, though quantities which are originally dimensionless are denoted by the original symbol. The dimensionless radial marker $x = \frac{r}{a}$ is used so the interior of the fluid sphere is described with $x \in [0, 1)$.

For the first model we get

$$\tilde{p}_r = \tilde{\alpha}_1 + \alpha_2 \tilde{\rho}, \quad (51)$$

$$\tilde{\rho} = \frac{\frac{1}{8\pi}[\tilde{f}(x) + \tilde{h}(x)] - \tilde{\alpha}_1}{1 + \alpha_2}, \quad (52)$$

$$\tilde{p}_r = \frac{\tilde{\alpha}_1 + \frac{\alpha_2}{8\pi}[\tilde{f}(x) + \tilde{h}(x)]}{1 + \alpha_2}, \quad (53)$$

$$\tilde{p}_t = \frac{\tilde{j}(x) + \tilde{h}(x) + \alpha_2[\tilde{j}(x) - \tilde{f}(x)] - 8\pi\tilde{\alpha}_1}{8\pi(1 + \alpha_2)}, \quad (54)$$

$$\tilde{E}^2 = \frac{8\pi\tilde{\alpha}_1 + \alpha_2\tilde{f}(x) - \tilde{h}(x)}{1 + \alpha_2}, \quad (55)$$

$$\tilde{\alpha}_1 = -\frac{\tilde{\rho}(1)\tilde{p}_r(0)}{\tilde{\rho}(0) - \tilde{\rho}(1)}, \qquad \alpha_2 = \frac{\tilde{p}_r(0)}{\tilde{\rho}(0) - \tilde{\rho}(1)}, \quad (56)$$

where

$$\tilde{f}(x) = e^{-\tilde{A}x^2}\left(2\tilde{A} - \frac{1}{x^2}\right) + \frac{1}{x^2}, \qu(57)$$

$$\tilde{h}(x) = e^{-\tilde{A}x^2}\left(2\tilde{B} + \frac{1}{x^2}\right) - \frac{1}{x^2}, \quad (58)$$

$$\tilde{j}(x) = \frac{e^{-\tilde{A}x^2}}{2}[2\tilde{B} + 2\tilde{B}^2x^2 + 2(\tilde{B} - \tilde{A}) - 2\tilde{A}\tilde{B}x^2], \quad (59)$$

$$\tilde{\rho}(0) = \frac{3\tilde{A}}{8\pi}, \quad (60)$$

$$\tilde{\rho}(1) = \frac{(\tilde{A} + \tilde{B})e^{-\tilde{A}}}{4\pi}, \quad (61)$$

$$\tilde{p}_r(0) = \frac{2\tilde{B} - \tilde{A}}{8\pi}, \quad (62)$$

$$\tilde{A} = a^2 A, \qquad \tilde{B} = a^2 B. \quad (63)$$

The second model is described with

$$\tilde{p}_r = \tilde{\beta}_1 + \frac{\tilde{\beta}_2}{\tilde{\rho}}, \quad (64)$$

$$\tilde{\rho} = \frac{\tilde{k}(x) - \tilde{\beta}_1 \pm \sqrt{[\tilde{k}(x) - \tilde{\beta}_1]^2 - 4\tilde{\beta}_2}}{2}, \quad (65)$$

$$\tilde{\beta}_1 = \frac{\tilde{\rho}(0)\tilde{p}_r(0)}{\tilde{\rho}(0) - \tilde{\rho}(1)}, \qquad \tilde{\beta}_2 = -\frac{\tilde{\rho}(0)\tilde{\rho}(1)\tilde{p}_r(0)}{\tilde{\rho}(0) - \tilde{\rho}(1)}. \quad (66)$$

For the third model we obtain

$$\tilde{p}_r = \gamma_1\tilde{\rho} + \frac{\tilde{\gamma}_2}{\tilde{\rho}}, \quad (67)$$

$$\tilde{\rho} = \frac{\tilde{k}(x) \pm \sqrt{\tilde{k}(x)^2 - 4(1 + \gamma_1)\tilde{\gamma}_2}}{2(1 + \gamma_1)}, \quad (68)$$

$$\gamma_1 = \frac{\tilde{\rho}(0)\tilde{p}_r(0)}{\tilde{\rho}(0)^2 - \tilde{\rho}(1)^2}, \qquad \tilde{\gamma}_2 = -\frac{\tilde{\rho}(0)\tilde{p}_r(0)\tilde{\rho}(1)^2}{\tilde{\rho}(0)^2 - \tilde{\rho}(1)^2}. \quad (69)$$

For models with nonlinear EOS, $\tilde{p}_t$ and $\tilde{E}^2$ are calculated with the dimensionless versions of (26) and (27), respectively.

From (49) we get

$$\tilde{E}(1)^2 = \chi^2 \quad (70)$$

which applies to the three models.

Finally, the dimensionless proper charge density is given by

$$\tilde{\sigma} = \frac{e^{-(\tilde{A}x^2/2)}}{4\pi x^2} \frac{d}{dx}(x^2\tilde{E}). \quad (71)$$

V. ANALYSIS OF THREE MODELS

We consider only external solutions (45) which exclude horizons. The standard analysis of the roots of $g_{00} = 0$ implies that the values of χ are restricted by the values of μ. Three cases arise:

(1) $\mu \in (0, 1)$, $2\mu - 1 < \chi^2 < \mu^2$;
(2) $\mu \in (0, 1)$, $\chi = \mu$;
(3) $\mu > 0$, $\chi > \mu$.

From Eqs. (20) and (46) we see that $\rho(0)$ is positive if and only if $2\mu - 1 < \chi^2 < 2\mu$, which we admit as an additional restriction on χ.

The geometric mass in (45) is given by $m = \frac{GM}{c^2}$, where G is the gravitational constant, M is the mass of the charged source, and c is the speed of light—all in conventional units. If the mass M of the charged star equals one solar mass and $a = 10$ Km, then $\mu = \frac{GM}{c^2 a} \approx 0.147$. Hence $2\mu - 1$ is negative and $\sqrt{2\mu} \approx 0.543$.

Using (60) and (62) the central density $\tilde{\rho}(0)$ and central pressure $\tilde{p}_r(0)$ can be evaluated for $\mu = 0.147$ and $\chi \in [0, 0.543)$. The monotonic decreases of these two parameters with increasing χ are shown in Figs. 1 and 2. We observe that $\tilde{p}_r(0)$ is positive only when χ takes values in the range $0 \leq \chi < \chi_0$, where $\chi = \chi_0$ is the only zero of $\tilde{p}_r(0)$ in the interval $\chi \in [0, 0.543)$. It is approximately given by $\chi_0 \approx 0.191$.

For fixed μ we see that $\tilde{\rho}(0)$, $\tilde{\rho}(1)$ and $\tilde{p}_r(0)$ depend only on χ. Hence Eqs. (56), (66), and (69) provide expressions for the EOS parameters as functions of χ. As shown in Figs. 3–5, $\tilde{\beta}_2(\chi) < 0$, $\gamma_1(\chi) > 0$ and $\tilde{\gamma}_2(\chi) < 0$ for $\mu = 0.147$ and $\chi \in [0, \chi_0)$. These results allow us to select the positive definite roots from (39) and (44), and discuss models with $\tilde{\rho}(x) > 0$.

For concreteness we carry out the numerical and graphical analysis of models with $\mu = 0.147$ and $\chi \in [0, \chi_0)$, characterized by positive matter density and positive pressur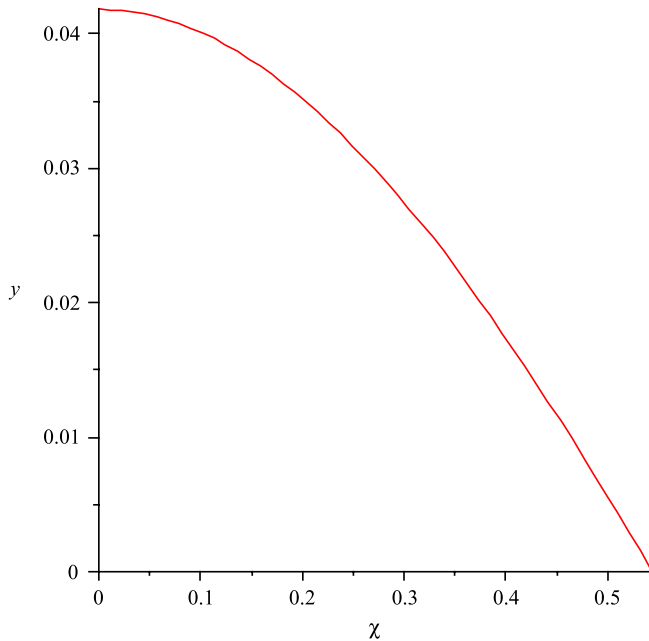e at $x = 0$. Clearly $\chi = 0$ describes sources with zero net charge. This condition is compatible with nonzero proper charge densities $\tilde{\sigma}(x)$. Higher values of χ are associated with increasingly repulsive electrostatic forces that affect pressure and matter density profiles. We aim to find out how the different forces that allow equilibrium configurations accommodate to varying net charge.

To begin with we examine sources with linear EOS and a selection of χ values. The corresponding profiles for matter

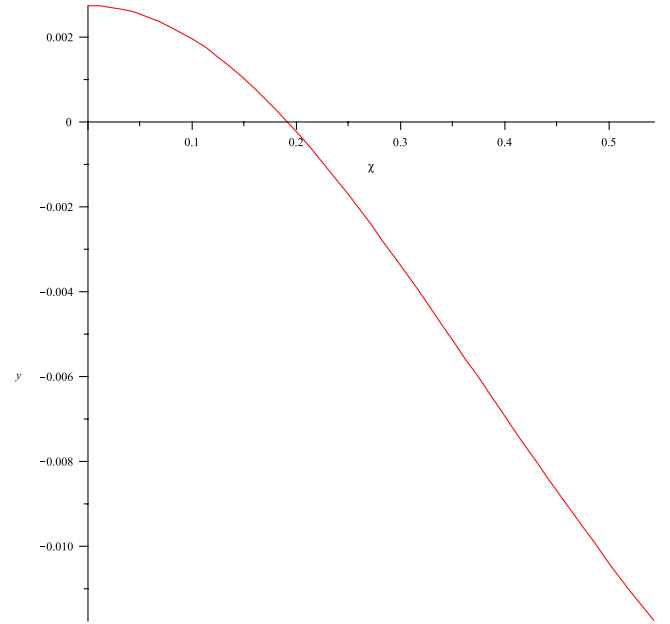FIG. 2 (color online).   Central pressure $\tilde{p}_r(0)$ as a function of χ for $\mu = 0.147$ [$y \equiv \tilde{p}_r(0)$].

FIG. 1 (color online).   Central density $\tilde{\rho}(0)$ as a function of χ for $\mu = 0.147$ [$y \equiv \tilde{\rho}(0)$].
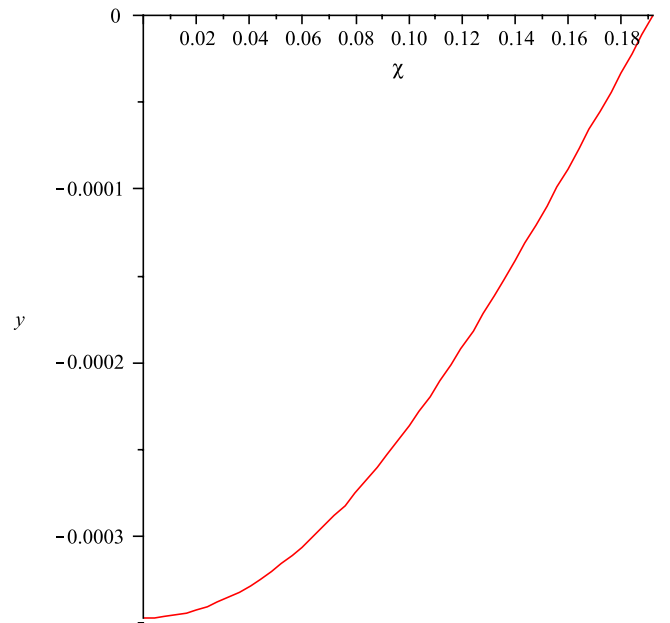

FIG. 3 (color online).   Coefficient $\tilde{\beta}_2$ as a function of χ for $\mu = 0.147$ ($y \equiv \tilde{\beta}_2$).
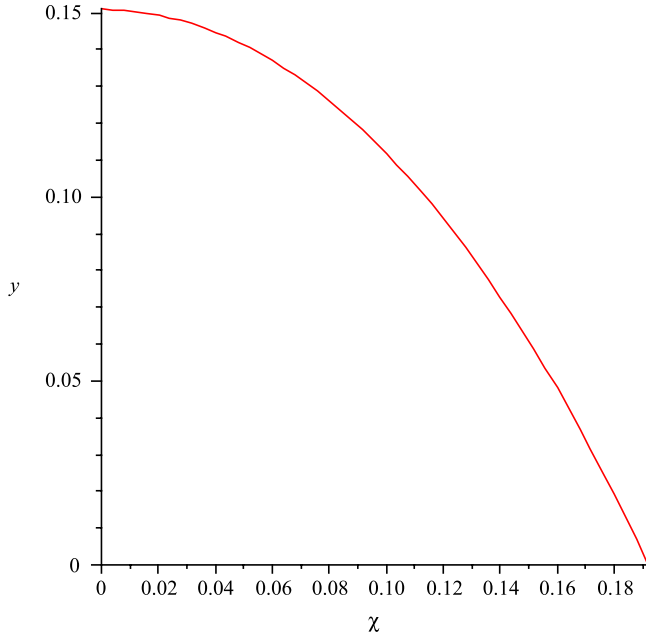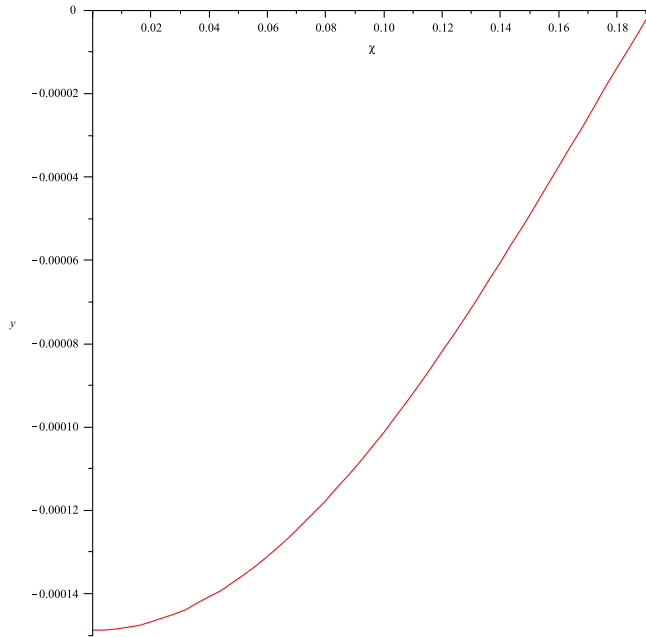
FIG. 4 (color online).   Coefficient $\tilde{\gamma}_1$ as a function of χ for $\mu = 0.147$ ($y \equiv \tilde{\gamma}_1$).
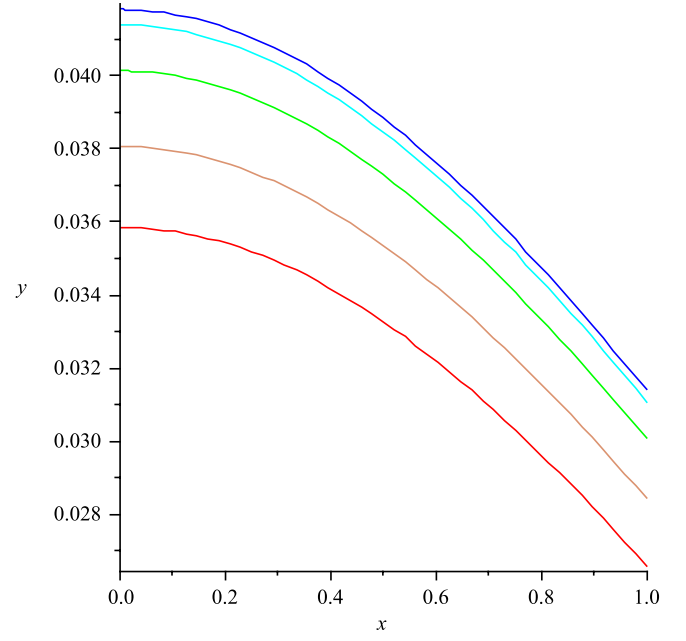

FIG. 6 (color online).   Matter density $\tilde{\rho}$ as a function of x for five different values of χ. In this figure, the curves 1-5 from the top (blue, cyan, green, tan, and red curves) correspond to $\chi = 0$, 0.05, 0.10, 0.15, and 0.19, respectively, ($y \equiv \tilde{\rho}$).

density, radial and tangential pressures, and electric field are displayed in Figs. 6–9. We observe decreasing values of matter density and pressure associated with increasing values of χ. Figure 9 shows electric field profiles satisfying $\tilde{E}(0) = 0$ and $\tilde{E}(1) = \chi$. Very large negative gradients of $\tilde{E}$ develop near the surface of the sphere for $\chi = 0$, and $\tilde{E}$ increases at every $x \in (0, 1]$ with increasing χ. Notably

Fig. 7 indicates that increasing net charges and electric fields are associated with decreasing radial pressure gradients at each point.
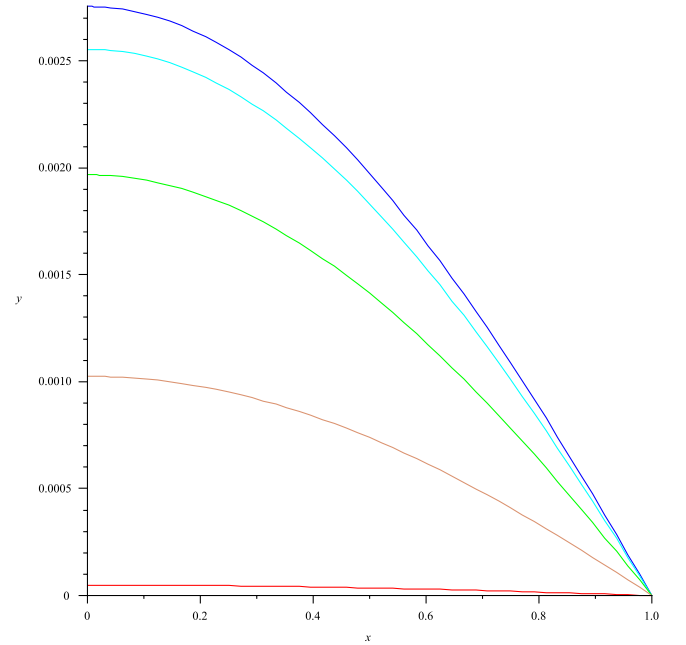

FIG. 5 (color online).   Coefficient $\tilde{\gamma}_2$ as a function of χ for $\mu = 0.147$ ($y \equiv \tilde{\gamma}_2$).

FIG. 7 (color online).   Radial pressure $\tilde{p}_r$ as a function of x for five different values of χ. In this figure, the curves 1-5 from the top (blue, cyan, green, tan, and red curves) correspond to $\chi = 0$, 0.05, 0.10, 0.15, and 0.19, respectively, ($y \equiv \tilde{p}_r$).
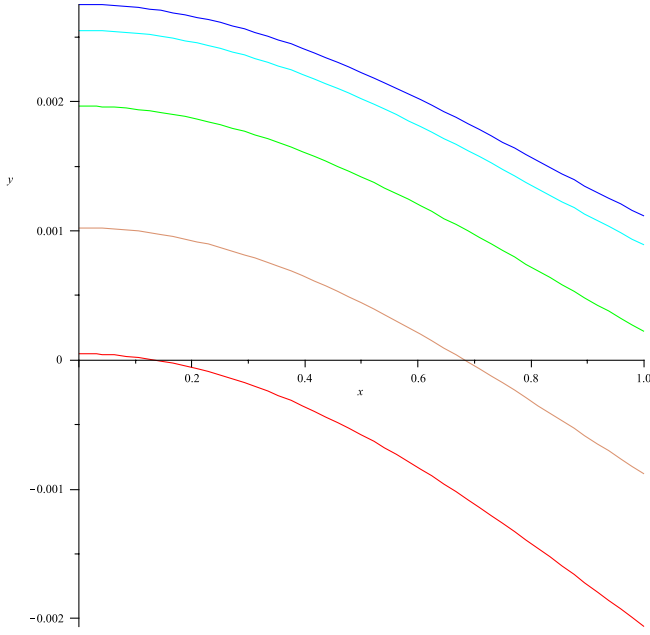
FIG. 8 (color online).   Tangential pressure $\tilde{p}_t$ as a function of x for five different values of χ. In this figure, the curves 1-5 from the top (blue, cyan, green, tan, and red curves) correspond to $\chi = 0$, 0.05, 0.10, 0.15, and 0.19, respectively, ($y \equiv \tilde{p}_t$).

FIG. 10 (color online).   Square of radial sound velocity v_{sr}^2 as a function of x for five different values of χ. In this figure, the curves 1-5 from the top (blue, cyan, green, tan, and red curves) correspond to $\chi = 0$, 0.05, 0.10, 0.15, and 0.19, respectively, ($y \equiv v_{sr}^2$).

Figures 10 and 11 show profiles for the squares of radial and tangential sound speeds, defined by $v_{sr}^2 = \frac{dp_r}{d\rho}$ and $v_{st}^2 = \frac{dp_t}{d\rho}$, respectively. We observe that v_{sr}^2 is independent of x and decreases with increasing χ. For fixed χ, v_{st}^2 monotonically decreases with increasing x; and increases with increasing χ for fixed x. These parameters satisfy the
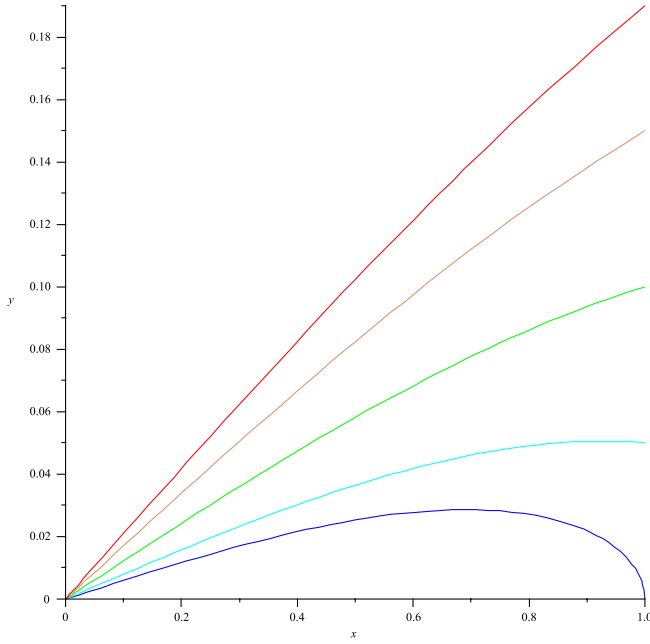

FIG. 9 (color online).   Electric field $\tilde{E}$ as a function of x for five different values of χ. In this figure, the curves 1-5 from the bottom (blue, cyan, green, tan, and red curves) correspond to $\chi = 0$, 0.05, 0.10, 0.15, and 0.19, respectively, ($y \equiv \tilde{E}$).
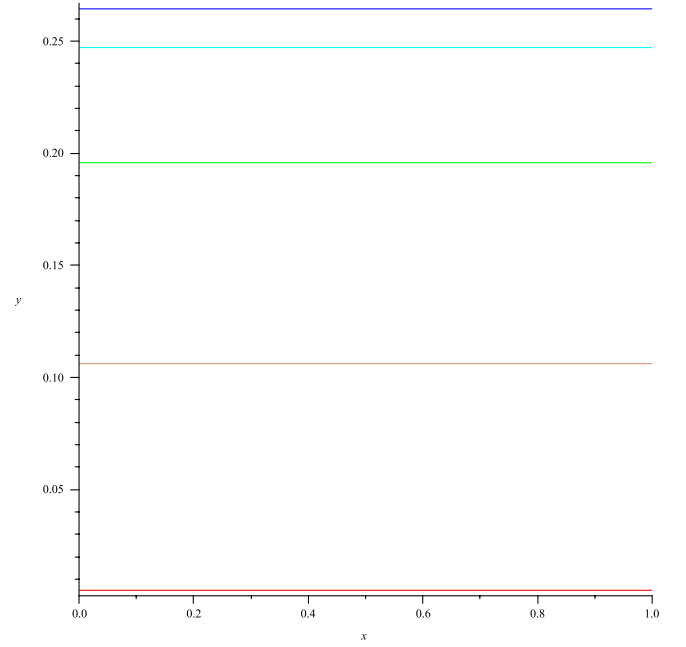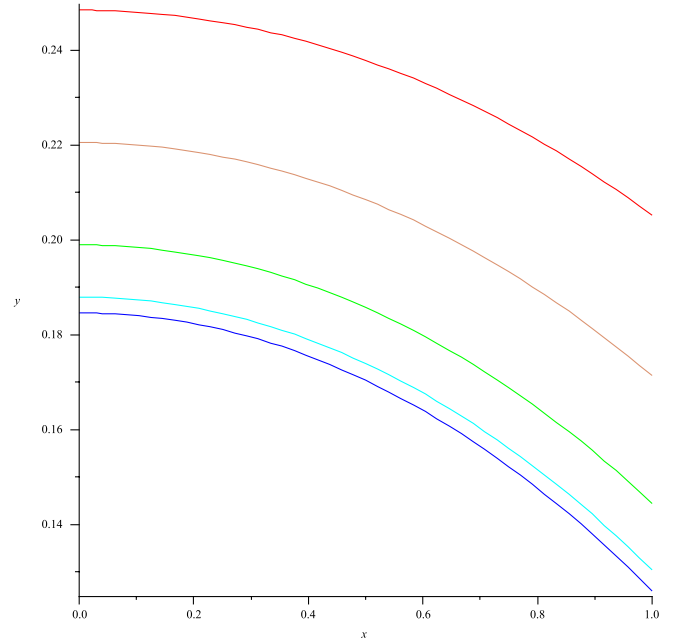

FIG. 11 (color online).   Tangential sound velocity v_{st}^2 as a function of x for five different values of χ. In this figure, the curves 1-5 from the bottom (blue, cyan, green, tan, and red curves) correspond to $\chi = 0$, 0.05, 0.10, 0.15, and 0.19, respectively, ($y \equiv v_{st}^2$).

inequalities $0 \leq v_{sr}^2 \leq 1$ and $0 \leq v_{st}^2 \leq 1$ everywhere within the charged fluid for the five values of χ considered.

Based on the standard analysis of energy conditions for charged anisotropic fluids (see, for example, [10]), we find that the weak energy condition (WEC), the strong energy condition (SEC) and the dominant energy condition (DEC) are simultaneously satisfied if and only if the following six inequalities hold at every point within the source:

$$\tilde{\rho} + \tilde{p}_r \geq 0, \tag{72}$$

$$\tilde{\rho} + \frac{\tilde{E}^2}{8\pi} \geq 0, \tag{73}$$

$$\tilde{\rho} + \tilde{p}_t + \frac{\tilde{E}^2}{4\pi} \geq 0, \tag{74}$$

$$\tilde{\rho} + \tilde{p}_r + 2\tilde{p}_t + \frac{\tilde{E}^2}{4\pi} \geq 0, \tag{75}$$

$$\tilde{\rho} + \frac{\tilde{E}^2}{8\pi} - \left| \tilde{p}_r - \frac{\tilde{E}^2}{8\pi} \right| \geq 0, \tag{76}$$

$$\tilde{\rho} + \frac{\tilde{E}^2}{8\pi} - \left| \tilde{p}_t + \frac{\tilde{E}^2}{8\pi} \right| \geq 0. \tag{77}$$

Inequalities (72) and (73) hold automatically for the sources considered here. Straightforward plotting of the left sides of (74)–(77) shows that these inequalities are satisfied as well at every $x \in [0, 1]$.

Further analysis shows that models with nonlinear EOS (64) and (67) are very similar to those satisfying (51). Particularly, matter densities and radial pressures are everywhere positive, matter densities as well as radial and tangential pressures monotonically decrease with increasing x, radial and tangential sound speeds satisfy $0 \leq v_{sr}^2 \leq 1$ and $0 \leq v_{st}^2 \leq 1$, v_{sr} decreases with increasing χ for fixed x, and WEC, SEC, and DEC are satisfied for $\mu = 0.147$ and $\chi = 0, 0.05, 0.1, 0.15, 0.19$. However, models with nonlinear EOS get v_{sr} profiles which increase monotonically with increasing x and fixed χ.

Another difference among the three models concerns the anisotropy parameter $\tilde{\Delta} = \tilde{p}_t - \tilde{p}_r$. As shown in Figs. 12–14, each EOS affect the dependence of $\tilde{\Delta}$ on x in a different way. Particularly, the sign of $\tilde{\Delta}$ is the same at every $x \in (0, 1]$ for fixed χ only in models with linear EOS. The effect of (64) on pressure anisotropy is notorious as three $\tilde{\Delta}(x)$ profiles develop sign changes in that case. However the predominance of radial pressure over tangential pressure for the highest value of χ is a common feature of the three models.

Are these three types of models physically meaningful? Delgaty and Lake found that only a relatively small number of proposed perfect fluid sources for the Schwarzschild metric satisfy a set of well established conditions for physical acceptability [12]. These conditions include regularity of the origin, positive matter density and pressure,
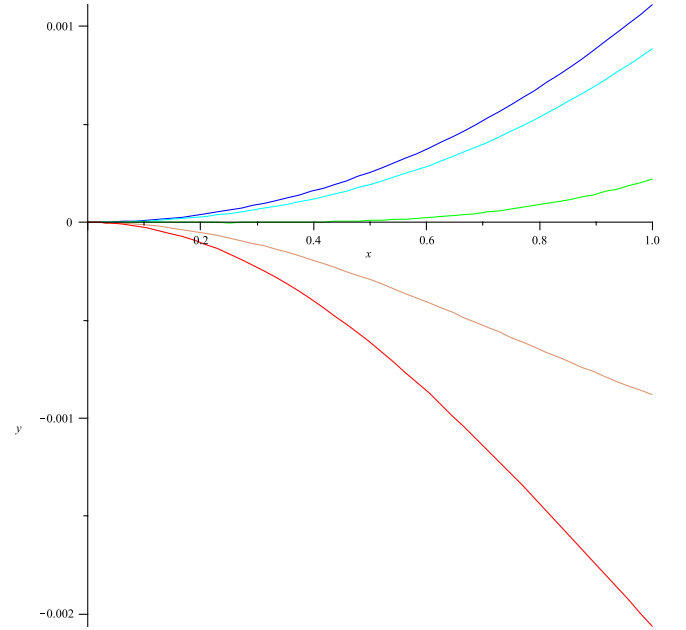

FIG. 12 (color online). Anisotropic parameter $\tilde{\Delta}$ for the first model as a function of x for five different values of χ. In this figure, the curves 1-5 from the top (blue, cyan, green, tan, and red curves) correspond to $\chi = 0, 0.05, 0.10, 0.15,$ and 0.19, respectively, ($y \equiv \tilde{\Delta}$).

decreasing matter density and pressure with increasing r, causal sound propagation, and smooth matching of the internal and external metrics at the fluid-vacuum interface
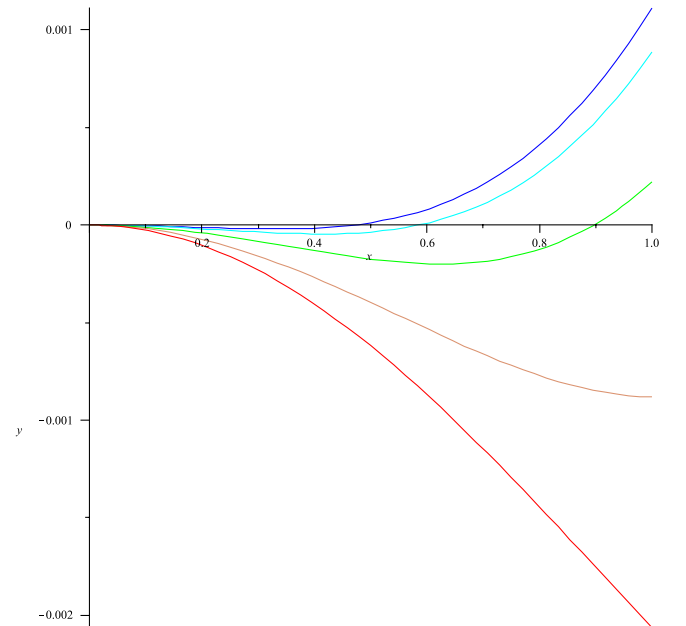

FIG. 13 (color online). Anisotropic parameter $\tilde{\Delta}$ for the second model as a function of x for five different values of χ. In this figure, the curves 1-5 from the top (blue, cyan, green, tan, and red curves) correspond to $\chi = 0, 0.05, 0.10, 0.15,$ and 0.19, respectively, ($y \equiv \tilde{\Delta}$).

FIG. 14 (color online).　Anisotropic parameter $\tilde{\Delta}$ for the third model as a function of x for five different values of χ. In this figure, the curves 1-5 from the top (blue, cyan, green, tan, and red curves) correspond to $\chi = 0$, 0.05, 0.10, 0.15, and 0.19, respectively, ($y \equiv \tilde{\Delta}$).
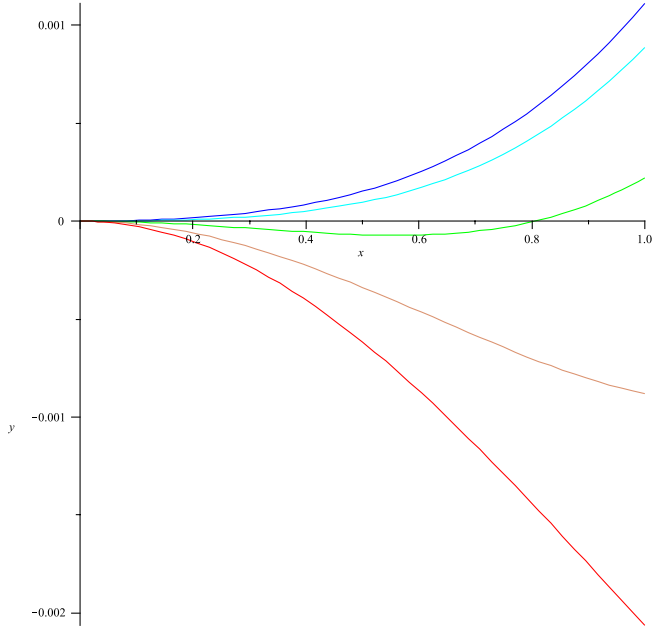

FIG. 15 (color online).　Proper charge density $\tilde{\sigma}$ as a function of $x \in [0, 0.999]$ for five different values of χ. In this figure, the curves 1-5 from the bottom (blue, cyan, green, tan, and red curves) correspond to $\chi = 0$, 0.05, 0.10, 0.15, and 0.19, respectively, ($y \equiv \tilde{\sigma}$).

($r = a$). Some authors add the condition of monotonically decreasing sound speed with increasing r (see, for example, [13]). Regarding anisotropic fluid sources, the causality condition $0 \leq v_s^2 \leq 1$ has been imposed on radial and tangential sound speeds (see, for example, [14,15]. Disagreement arises in connection with the sign of tangential pressure which is unrestricted for some authors (see, for example, [14]) and strictly positive for others (see, for example, [15]). The above discussion indicates that our three charged anisotropic sources satisfy most of the usual acceptability criteria. Conflict may arise only in connection with negative tangential pressures occurring for the highest χ values, constant sound speeds v_{sr} associated with the linear EOS, and the increase of v_{sr} with increasing x appearing in the models with nonlinear EOS.

Electric interactions and charge distributions in our models deserve further analysis. We have found that $\tilde{E}$ profiles are affected by the choice of EOS. Particularly, in models with $\chi = 0$ the maximum $\tilde{E}$ values are approximately 0.03, 0.07, and 0.05, corresponding to (51), (64), and (67), respectively. In the case of EOS (51), $\tilde{\sigma}(0)$ is finite and increases with increasing χ; and $\tilde{\sigma}(1)$ is finite for $\chi = 0.05$, 0.1, 0.15, 0.19 but unbounded for $\chi = 0$. Moreover, only sources with $\chi = 0$ contain electric charge of both signs. We could have anticipated this behavior of $\tilde{\sigma}$ from Maxwell Eq. (71) and the slope changes displayed in Fig. 9. Figure 15 shows the arising $\tilde{\sigma}$ profiles in the restricted interval [0,0.999]. The most important difference among $\tilde{\sigma}$ profiles associated with the three EOS is that
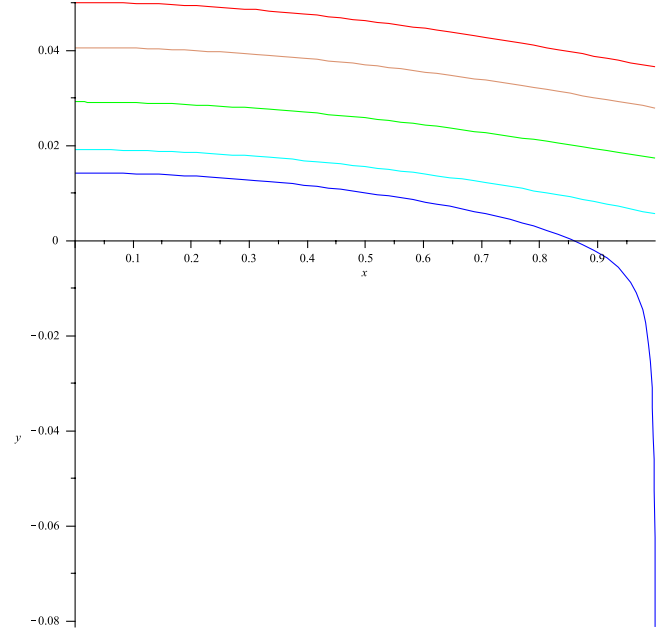
models with nonlinear EOS and $\chi = 0.05$ also involve positive and negative electric charges.

We have noticed that the charge distributions considered by Thirukkanesh and Maharaj [5] are singular at the origin, where the electric field does not vanish. Alternatively, all our sources have vanishing electric field and finite proper charge density at $r = 0$. On the other hand, our models with $\chi = 0$ involve charge distributions that are singular at the fluid-vacuum interface. We remark that charged thin shells are not considered in our study and electric fields are continuous at $r = a$. Also, charged sources with $\chi = 0$ are characterized by $E(a) = 0$ and unbounded $\lim_{r \to a^-} E'(r)$. Arbitrarily large electric field gradients near the fluid-vacuum are puzzling and we proceed with a preliminary discussion of their significance.

The proper charge density σ appears explicitly in the inhomogeneous Maxwell Eq. (5). It determines the net charge inside a sphere of radius r through the formula

$$q(r) = 4\pi \int_0^r \sigma(r) e^{\lambda(r)/2} r^2 dr. \qquad (78)$$

We remark that $q(a)$ is the total charge of the source, denoted by q in (45). It is $q(r)$ the quantity that actually determines the electric field

$$E(r) = \frac{q(r)}{r^2}. \qquad (79)$$

Proper charge density $\sigma(r)$ is not an observable quantity in standard EM theory. We have seen that $E(r)$ takes part in

the formulation of the energy conditions of general relativity through the contribution of the Maxwell field to the energy-momentum tensor. In contrast, the authors are not aware of any condition for physical acceptability imposed directly on σ.

Both spacetime curvature and electric field gradients deviate the world lines of charged test particles. Balkin, van Holten, and Kerner [16] and van Holten [17] have derived covariant formulas for the relative acceleration of particles with the same charge/mass ratio. Their equations include terms containing derivatives of the Maxwell tensor. The question arises as to whether these terms could lead to infinite relative accelerations for pairs of charged test particles passing through the fluid-vacuum interface of models with $\chi = 0$. Hence very large relative accelerations of test particles could allow indirect observation of infinite charge density located at the vacuum-fluid interface of our sources.

The fundamental invariant of the electromagnetic field $I_1 = F_{\mu\nu}F^{\mu\nu}$ has been used in the analysis of genuine singularities of static solutions for the Einstein-Maxwell equations [18]. This invariant is bounded at the fluid-vacuum interfaces of our three types of models. The inhomogeneous Maxwell equation implies that $I_2 = F^{\mu\nu}_{\ ;\nu}F^{\omega}_{\ \mu;\omega}$ is proportional to $\sigma(r)^2$. The fact that $\sigma(r)$ is unbounded at $r = a$ in models with $\chi = 0$ determines the singular behavior of a differential invariant of the theory. Questions about physical acceptability of solutions with regular I_1 and singular I_2 are analogous to those regarding spacetimes with regular curvature invariants and singular differential invariants discussed by Musgrave and Lake [19].

The discussion of physical acceptability for sources with zero net charge points at the equilibrium condition for sections with infinite charge density. Fluid elements with unbounded σ are located at $r = a$, where the electric field vanishes due to the choice $\chi = 0$. Nevertheless, the conclusion that no electric force acts on elements of charged fluid with infinite σ is not straightforward and deserves closer examination. Other features of our models motivate further analysis of equilibrium conditions. For example, as we keep μ constant and increase χ, repulsive electric forces increase with decreasing matter density, decreasing pressure, and decreasing radial pressure gradients. The question is, how gravitational and other fluid forces counteract increasing electrostatic repulsion when the charged fluid becomes more diluted and pressure gradients tend to vanish? The situation is clarified using the generalized Tolman-Oppenheimer-Volkov (TOV) equation as presented by Ponce de León [10]. (See also [20].) It reads

$$-\frac{M_G(\rho + p_r)}{r^2}e^{(\lambda-\nu)/2} - \frac{dp_r}{dr} + \sigma\frac{q}{r^2}e^{\lambda/2} + \frac{2}{r}(p_t - p_r)$$
$$= 0, \quad (80)$$

where $M_G = M_G(r)$ is the effective gravitational mass in-

side a sphere of radius r and $q = q(r)$ is given by (78). The effective gravitational mass is given by the expression

$$M_G(r) = \tfrac{1}{2}r^2 e^{(\nu-\lambda)/2}\nu', \quad (81)$$

derived from the Tolman-Whittaker formula and the Einstein-Maxwell equations [10].

Equation (80) expresses the equilibrium condition for charged fluid elements subject to gravitational, hydrostatic and electric forces, plus another force due to pressure anisotropy. Combined with (10), (11), (63), and (79), it takes the adimensional form

$$\tilde{F}_g + \tilde{F}_h + \tilde{F}_e + \tilde{F}_a = 0, \quad (82)$$

where

$$\tilde{F}_g = -\tilde{B}x(\tilde{\rho} + \tilde{p}_r), \quad (83)$$

$$\tilde{F}_h = -\frac{d\tilde{p}_r}{dx}, \quad (84)$$

$$\tilde{F}_e = \tilde{\sigma}\tilde{E}\,e^{(\tilde{A}x^2/2)}, \quad (85)$$

$$\tilde{F}_a = \frac{2}{x}(\tilde{p}_t - \tilde{p}_r). \quad (86)$$

The profiles of $\tilde{F}_g$, $\tilde{F}_h$, $\tilde{F}_e$, and $\tilde{F}_a$ for sources with linear EOS, $\mu = 0.147$ and $\chi = 0$ are shown in Fig. 16. Notably, the electric force acting on fluid elements with unbounded
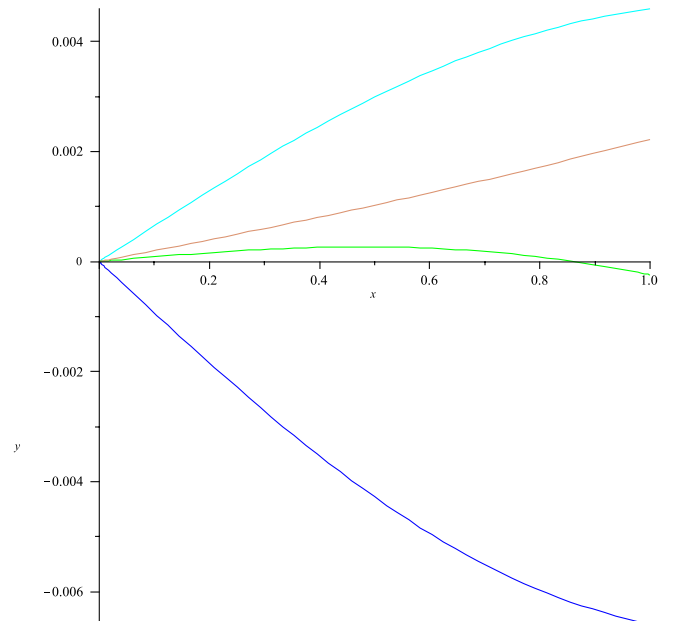

FIG. 16 (color online). Four different forces acting on fluid elements in static equilibrium as functions of x for $\mu = 0.147$ and $\chi = 0$. In this figure the curves 1–4 from the bottom (blue, green, tan, cyan curves) correspond to $\tilde{F}_g$, $\tilde{F}_e$, $\tilde{F}_a$, and $\tilde{F}_h$ respectively. The dummy variable y on the vertical axis represents any of these forces.
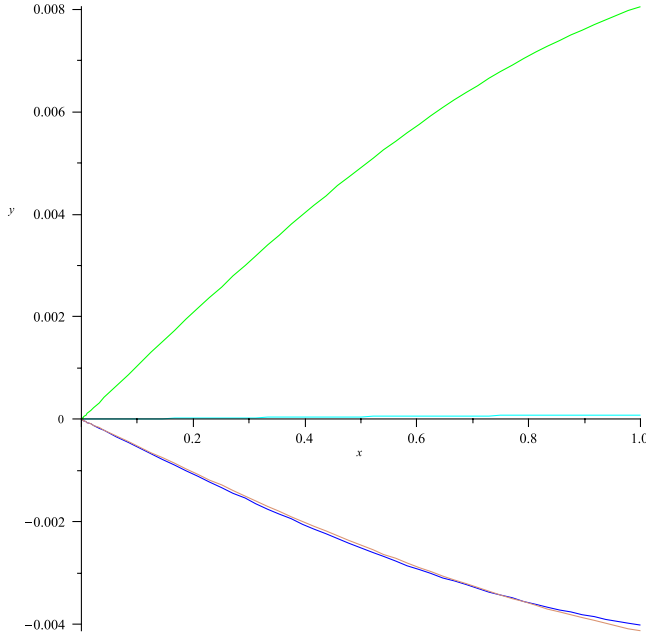
FIG. 17 (color online). Four different forces acting on fluid elements in static equilibrium as functions of x for $\mu = 0.147$ and $\chi = 0.19$. In this figure the first (green) and second (cyan) curves from the top correspond to $\tilde{F}_e$ and $\tilde{F}_h$, respectively. The third (tan) and fourth (blue) curves intersect at $x \approx 0.75$ and represent $\tilde{F}_a$ and $\tilde{F}_g$, respectively. The dummy variable y on the vertical axis represents any of these forces.

$\tilde{\sigma}$ located at $x = 1$ is finite although $\tilde{E}(1) = 0$ in this case. Equivalently $\lim_{x \to 1} \tilde{\sigma} \tilde{E}$ is finite. Furthermore, $\tilde{F}_e$ is the weakest force and changes sign at $x \approx 0.85$. Both $\tilde{F}_h$ and $\tilde{F}_a$ point outwards at every $x \in (0, 1]$. Electric forces increase and radial pressure gradients decrease with increasing χ. When $\chi = 0.19$ the hydrostatic force $\tilde{F}_h$ is relatively insignificant and $\tilde{F}_a$ points inwards, acting in conjunction with gravitational attraction to compensate the electrostatic repulsion. This situation is described in Fig. 17. Clearly, the sign of $\tilde{F}_a$ changes due to the predominance of p_r over p_t for the largest χ values. This sign inversion is essential for the configuration of our static, charged anisotropic sources with linear EOS.

We have extended the analysis of these four forces to models with nonlinear EOS and found essentially the same equilibrium configuration discussed above for linear EOS and $\chi = 0.19$. Particularly, $\tilde{F}_h$ is comparatively small, $\tilde{F}_g$ and $\tilde{F}_a$ have nearly the same profile and jointly counteract the electrostatic repulsion. Hence the choice of EOS has a negligible effect on the compensation of relatively large electrostatic repulsion by gravitational attraction and pressure anisotropy.

Equations (2)–(5) indicate that matter density, radial pressure, tangential pressure, and electric field strength affect the spacetime metric in our relativistic fluid models. Our choice $\mu = 0.147$ corresponds to a compact stellar object ($M = 2 \times 10^{33}$ g, $a = 10^6$ cm), so pressure is ex-

pected to play a substantial role here. The question arises as to whether the electrostatic energy density significantly contributes to the source of gravity. We compute dimensionless values of the physical variables and get maxima and minima for $\tilde{\rho}_0$ (central matter density), $\tilde{p}_0$ (central pressure), $\tilde{p}_{\text{ta}}$ (tangential pressure at $r = a$), and $\tilde{E}_a^2$ (electrostatic energy density at $r = a$) as well as $\tilde{E}_m^2$ (maximum electrostatic energy density for $\chi = 0$). Approximate numerical results for the model with linear EOS are displayed in Table I.

We observe that the maximum values of $\tilde{p}_0$ and $\tilde{p}_{\text{ta}}$ are just 1 order of magnitude smaller than the maximum of $\tilde{\rho}_0$. These maxima correspond to the source with $\chi = 0$ i.e. zero net charge and weakest electrostatic repulsion. Notably, these density and pressure values are very similar to the dimensionless density $\tilde{\rho}_s$ and dimensionless central pressure $\tilde{p}_{0s}$ of the (uncharged) Schwarzschild internal solution (SIS) with the same μ value. Using well-known formulas for the SIS in geometrized units [21], we derive the dimensionless expressions

$$\tilde{\rho}_s = \frac{3\mu}{4\pi}, \qquad (87)$$

$$\tilde{p}_{0s} = \frac{3\mu^2}{8\pi}, \qquad (88)$$

leading to the approximate results $\tilde{\rho}_s = 0.036$ and $\tilde{p}_{0s} = 0.003$.

The value of $\tilde{E}_m^2$ shown in Table I indicates a substantial contribution of the Maxwell field to the source of gravity in the case of zero net charge, although matter density and pressure predominate.

In sources with maximum net charge ($\chi = 0.19$) $\tilde{p}_0$ decreases in 2 orders of magnitude, $\tilde{p}_{\text{ta}}$ doubles its absolute value and gets the opposite sign, and $\tilde{\rho}_0$ and $\tilde{E}_a^2$ have the same approximate value. From Figs. 13 and 14 we see that the reduction of radial pressure with increasing net charge makes gravitational attraction weaker in spite of the larger values of electrostatic energy density. We have discussed above that the sign inversion of tangential pressure leads to an extra force which complements gravitational attraction, so that the stronger electric repulsion gets compensated. Certainly static equilibrium is attainable in these charged sources thanks to pressure anisotropy.

The discussion of the above quantities in conventional units is interesting as well. Adimensional density and pressure values are expressed in geometrized units and then converted to cgs units using well-known conversion

TABLE I. Dimensionless values of physical variables for the model with linear EOS.

χ	$\tilde{\rho}_0$	$\tilde{p}_0$	$\tilde{p}_{\text{ta}}$	$\tilde{E}_a^2$	$\tilde{E}_m^2$
0	0.042	0.003	0.001	0	0.0009
0.19	0.036	0.000 05	-0.002	0.036	$\cdots$

TABLE II. Density and pressures for the model with linear EOS expressed in cgs units.

χ	ρ_0 (gr/cm^3)	p_0 (dyn/cm^2)	p_{ta} (dyn/cm^2)
0	5.6×10^{14}	3.6×10^{34}	1.2×10^{34}
0.19	4.8×10^{14}	6×10^{32}	-2.4×10^{34}

TABLE III. Electric field strengths and net charge for the model with linear EOS expressed in Gaussian-cgs units.

χ	E_a (statvolt/cm)	E_m (statvolt/cm)	q (statcoul)
0	0	3.7×10^{23}	0
0.19	2.3×10^{24}	$\cdots$	1.9×10^{29}

factors [22]. Similarly, adimensional values of electrical variables are expressed in geometrized units, then converted to Heaviside-Lorentz units and finally to Gaussian-cgs units. The corresponding results are displayed in Tables II and III.

These values of central matter density and pressure as well as electric field strength and net charge in conventional units are similar to those discussed by previous authors in the context of charged compact objects with isotropic pressure [23]. It is understood that the huge gravitational attraction determined by these values of central matter density and pressure compensates repulsive electrostatic forces associated with field strengths and net charges with orders of magnitude 10^{24} statvolt/cm (10^{26} V/cm) and 10^{29} statcoul ($10^{19}C$), respectively. However, our study of charged anisotropic sources points at the crucial role that forces caused by pressure anisotropy can play in the construction of equilibrium states. This anisotropic effect is equally important for the three models considered here, at least for the assumed value of $\mu = 0.147$. Provided that pressure anisotropy supplies an inward-directed force that compensates electrostatic repulsion, we expect our sources can achieve higher charges and electric field strengths than sources with isotropic pressures and the same μ value. Also, our results for sources with zero net charge suggest a possible role for pressure anisotropy and electric charge in the structure of static sources for the external Schwarzschild metric.

VI. CONCLUDING REMARKS

The linear equation (32) links our analytical approach with the numerical treatment of electrically charged strange quark stars by Negreiros et al. [24] based on the MIT bag model. They also assume (18) and impose vanishing isotropic pressure at the fluid-vacuum interface.

We have borrowed nonlinear EOS (38) (with $n = 1$) and (42) from current models of dark matter and dark energy. Most applications of Chaplygin and modified Chaplygin gases are cosmological and describe nonstatic, neutral gravitational fluids with isotropic pressures. Instead, our bounded sources involve static, asymptotically flat spacetimes and charged anisotropic fluids. Actually we have targeted the effects of these EOS on the interior regions and fluid-vacuum interfaces of charged stars apart from any cosmological framework. The question arises as to how dark matter-dominated star interiors could get electric charge. Specific charge transfer mechanisms hypothesized in studies of charged neutron stars [25] could be considered. Alternatively, a fraction of dark matter could be made up by massive particles with electric charge (CHAMPs) [26], so dark stars could be charged. We remark that our procedures and results are totally independent of any charge generation mechanism.

Lobo initiated the study of van der Waals (VDW) quintessence stars [27]. Apart from variations of ρ and p_r in the interior of the VDW fluid, which may be caused by gravitational instabilities, this author imposes a cut-off of the energy-momentum tensor at $r = a$, where the internal metric matches the external Schwarzschild solution. Again, the motivation for introducing this new type of bounded source is cosmological. Provided that the quintessence EOS leads to interesting descriptions of the late universe, stellar objects arising from fluid nucleation through density perturbations are explored.

The extended KB approach can be applied to a sphere of charged quintessence fluid. Apart from the hypothetical link of dark matter with CHAMPs, we cannot justify the introduction of charge in this model. However, we aim to test the applicability of the present approach against the more complicated VDW EOS

$$p_r = \frac{\delta_1 \rho}{1 - \delta_3 \rho} - \delta_2 \rho^2, \qquad (89)$$

which describes dark matter and dark energy as a single fluid [27].

Assuming that the interior metric is joined to (45), and that the electric field and radial pressure vanish at $r = 0$ and $r = a$ respectively, we evaluate (89) at the center and boundary of the charged sphere and solve two linear equations for δ_1 and δ_2 as functions of $\rho(0)$, $\rho(a)$, $p_r(0)$, and δ_3. Then (89) is combined with (31) to obtain

$$\delta_2 \delta_3 \rho^3 - (\delta_2 + \delta_3)\rho^2 + [1 + \delta_1 + \delta_3 g(r)]\rho - g(r) = 0, \qquad (90)$$

where $g(r) = \frac{f(r) + h(r)}{8\pi}$.

We do not go further into the analysis of the real roots of (90) and the corresponding sources. However, we anticipate difficulties in the selection of μ, χ, and $\tilde{\delta}_3$ values leading to positive definite matter densities.

The analysis of stability is beyond the scope of this paper. Results presented by Andréasson [28] regarding stability properties of charged anisotropic spheres could shed light on this fundamental issue. We highlight the

potentially interesting study of gravitational collapse of sources with zero net charge, and hope our results will motivate further research on these topics.

Finally, we point out that different EOS could be matched at specific radii to provide composite models. For example, a linear interior (core) with a nonlinear exterior (layer) matched at a location inside the charged fluid sphere might provide a better model than a simple EOS throughout. Using the extended KB approach developed here, both the core and the layer would be described with the same general metric (1) and the *ansätze* (10) and (11) with presumably different values of *A*, *B*, and *C* in each region. Less restricted choices of these constants could lead to charged thin shells emerging at the interface between the fluids.

[1] B. V. Ivanov, Phys. Rev. D **65**, 104001 (2002).
[2] R. Sharma and S. D. Maharaj, Mon. Not. R. Astron. Soc. **375**, 1265 (2007).
[3] B. W. Bonnor, Z. Phys. **160**, 59 (1960).
[4] D. Horvat, S. Ilijić, and A. Marunović, Classical Quantum Gravity **26**, 025003 (2009).
[5] S. Thirukkanesh and S. D. Marahaj, Classical Quantum Gravity **25**, 235001 (2008).
[6] K. D. Krori and J. Barua, J. Phys. A **8**, 508 (1975).
[7] K. Lake and P. Musgrave, Gen. Relativ. Gravit. **26**, 917 (1994).
[8] O. Bertolami and J. Páramos, Phys. Rev. D **72**, 123512 (2005).
[9] M. Jamil, U. Farooq, and M. A. Rashid, Eur. Phys. J. C **59**, 907 (2009).
[10] J. Ponce de León, Gen. Relativ. Gravit. **25**, 1123 (1993).
[11] G. J. G. Junevicus, J. Phys. A **9**, 2069 (1976).
[12] M. S. R. Delgaty and K. Lake, Comput. Phys. Commun. **115**, 395 (1998).
[13] J. Burke and D. Hobill, arXiv:0910.3230.
[14] T. Harko and M. K. Mak, Ann. Phys. (Leipzig) **11**, 3 (2002).
[15] H. Abreu, H. Hernandez, and L. A. Nunez, Classical Quantum Gravity **24**, 4631 (2007).
[16] A. Balakin, J. W. van Holten, and R. Kerner, Classical Quantum Gravity **17**, 5009 (2000).
[17] J. W. van Holten, arXiv:hep-th/0201083.
[18] J. B. Hartle and S. W. Hawking, Commun. Math. Phys. **26**, 87 (1972).
[19] P. Musgrave and K. Lake, Classical Quantum Gravity **12**, L39 (1995).
[20] We note that TOV equations have been used in the context of neutral Chaplygin stars and wormholes by V. Gorini, U. Moschella, A. Yu. Kamenshchik, V. Pasquier, and A. A. Starobinsky, Phys. Rev. D **78**, 064064 (2008); V. Gorini, A. Yu. Kamenshchik, U. Moschella, O. F. Piattella, and A. A. Starobinsky, Phys. Rev. D **80**, 104038 (2009).
[21] R. Wald, *General Relativity* (The University of Chicago Press, Chicago, 1984).
[22] C. W. Misner, K. S. Thorne, and J. A. Wheeler, *Gravitation* (Freeman, San Francisco, 1973)
[23] S. Ray, A. L. Espindola, M. Malheiro, and J. P. S. Lemos, Phys. Rev. D **68**, 084004 (2003).
[24] R. P. Negreiros, F. Weber, M. Malheiro, and V. Usov, Phys. Rev. D **80**, 083006 (2009).
[25] M. K. Mak, P. N. Dobson, and T. Harko, Europhys. Lett. **55**, 310 (2001).
[26] F. J. Sánchez-Salcedo, E. Martínez-Gómez, and J. Magaña, J. Cosmol. Astropart. Phys. 02 (2010) 031.
[27] F. S. N. Lobo, Phys. Rev. D **75**, 024023 (2007).
[28] H. Andréasson, Commun. Math. Phys. **288**, 715 (2009).